Robotics Traveling Van

Engineering Calculations Summary

Freddy Rivera – Project Manager
Colin Parsinia – Manufacturing Lead
Florence Fasugbe – Design Lead
Andrés Gonzales – Systems Lead

Fall 2025 -Spring 2026

Project Sponsor: Dr. Micheal Shafer
Faculty/Instructor: Professor David Willy
Sponsor Mentor: Sethuprasad Gorantla

Top Level Summary

Robot 1

The core challenge of this project is to achieve autonomous balance for an inherently unstable inverted pendulum robot. Because the center of mass is located above the pivot point, gravity continuously acts to pull the system into a state of collapse. Solving this requires a high-speed feedback PID loop that can detect minute angular deviations via high-resolution magnetic encoders and execute rapid restorative maneuvers using four DC gear motors. Beyond basic balance, the problem necessitates managing extreme electrical transients, reaching peaks of 13.1A, while ensuring that the resulting voltage sag does not disrupt the sensitive RP2040 logic. Our objective is to synchronize precision sensing, software-defined safety constraints, and robust power delivery to maintain stability without triggering thermal failure or system brownouts.

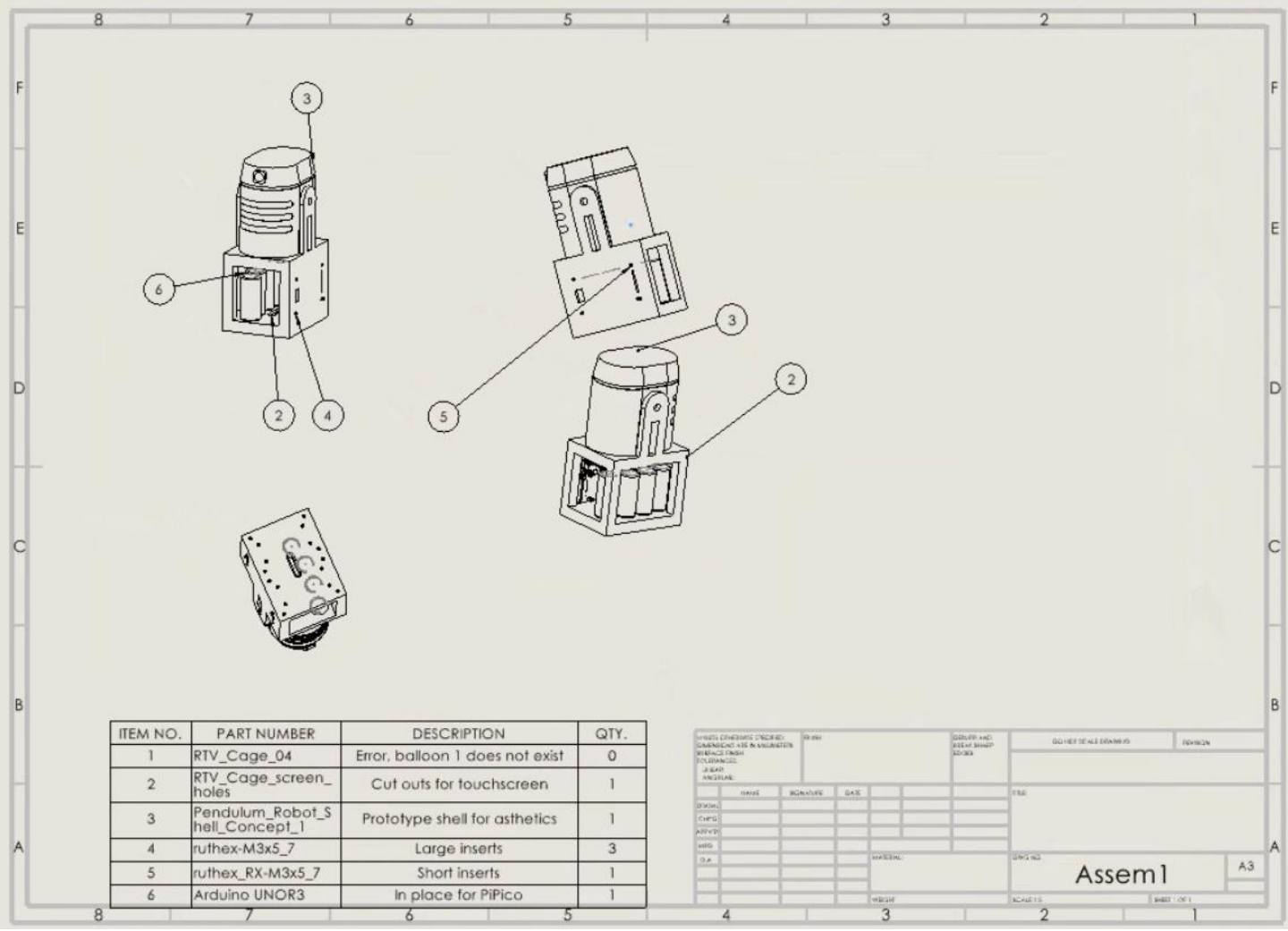

ITEM NO.	PART NUMBER	DESCRIPTION	QTY.
1	RTV_Cage_04	Error, balloon 1 does not exist	0
2	RTV_Cage_screen_holes	Cut outs for touchscreen	1
3	Pendulum_Robot_Shell_Concept_1	Prototype shell for asthetics	1
4	ruthex-M3x5_7	Large inserts	3
5	ruthex_RX-M3x5_7	Short inserts	1
6	Arduino UNOR3	In place for PiPico	1

Robot 2

Robot 2 is a *ball-on-beam stabilization system* intended as an educational demonstration platform for K–12 outreach. The objective of this robot is to dynamically stabilize a rolling ball along a trough-styled beam using closed-loop feedback control. This allows students to visually observe fundamental concepts in controls, dynamics, and sensing.

The current design consists of a *single rotating beam* driven about a central pivot axis by a stepper motor. The ball's position along the beam is analyzed by using a distance sensor, and beam angle is controlled through precise motor actuation. The system is designed to be robust, visually neat, and

modular to allow for repeated demonstrations and limitless classroom interactions. *Figure 2* shows the current top-level CAD model sketch of Robot 2 with major subsystems labeled.

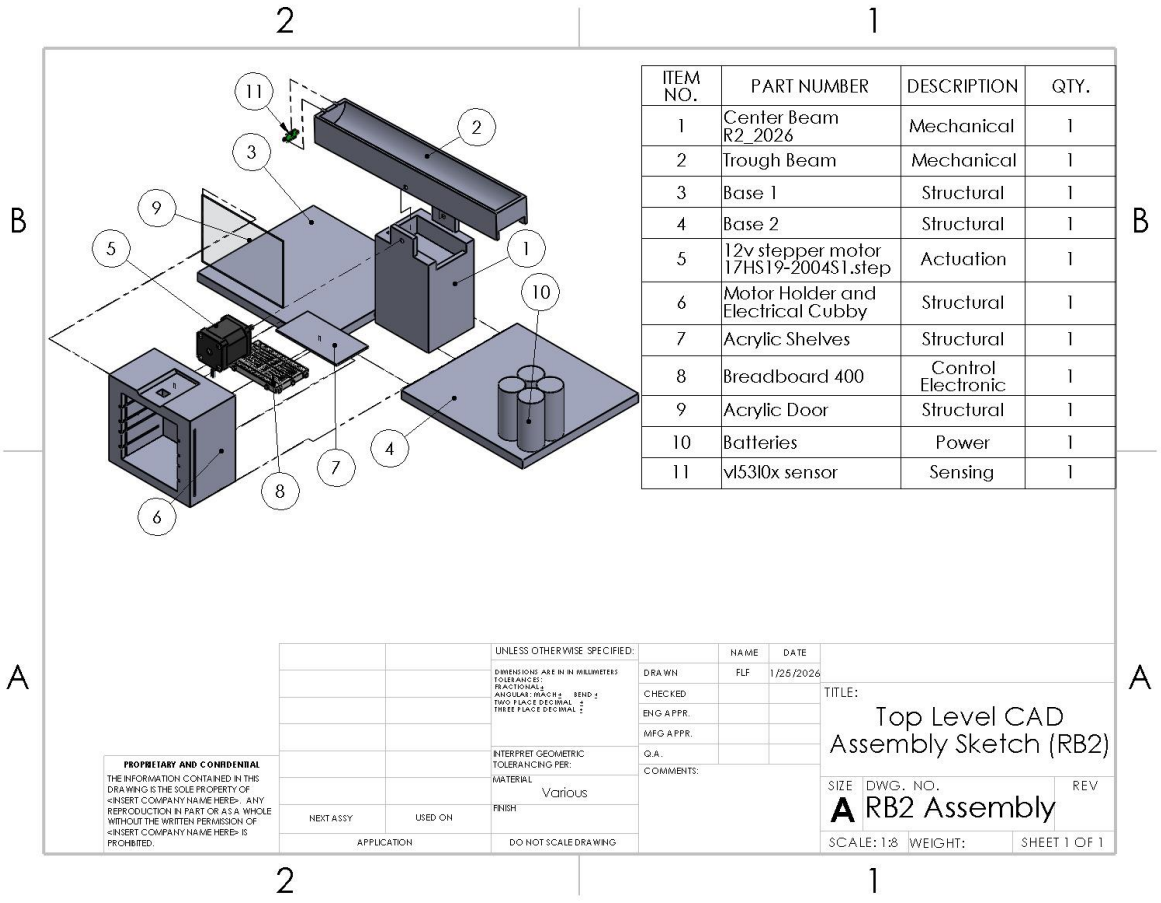

Figure 1: The top-level CAD assembly sketch with sub-systems being identified for robot 2.

Primary subsystems include:

1. Mechanical Structure: Parts of the robot that interact with other parts of the system dynamically.
    a. Trough beam
    b. Center beam holder
2. Structural: Provides mechanical support and the visualization of the system.
    a. Base
    b. Motor Holder and Electrical Cubby
    c. Shelves
    d. Door
3. Actuation: Physical movement based on the control signals.
    a. Stepper motor mounted at the beam's center pivot axis
4. Sensing: Distance sensor used to determine ball position along the beam.
    a. ToF Sensor
5. Control Electronics: Reads the ball's position and process the signals to make decisions.
    a. Micro-controller
    b. Stepper motor driver
    c. Supporting electronics (Breadboard)
6. Power System: Storing, regulating, and distributing electrical energy to the robot's electrical components.
    a. Rechargeable battery
    b. Voltage regulation hardware

These subsystems are integrated to form a single closed-loop control system where sensor feedback informs motor actuation to maintain or reposition the ball along the beam.

Summary of Standards, Codes, and Regulations

Robot 1

Given that the interface between the metal motors and the 3D-printed chassis holdthe primary mechanical risk, we have integrated brass heat-set inserts to maximize joint integrity. Our design is informed by ASME B18.2.8 for clearance hole diameters and ASME B1.13M for metric screw thread profiles, ensuring precise tolerances within our CAD model [1 & 2]. The M3 fastener is our primary hardware standard. We utilize 10mm screws in conjunction with deep-set threaded inserts to distribute high torque loads at the motor mounts. Similarly, we utilize 5mm screws with smaller threaded-inserts for low-stress mounting of the logic components and the 4” touchscreen, ensuring a secure fit without compromising the thinner sections of the printed geometry.

In terms of safety and interaction with our target audience, we have identified the pendulum's kinetic energy as a Class 2 Mechanical Source and implemented a dual-layer safeguard. To mitigate risks inherent in a mobile pendulum system, the design implements a "Safety by Separation" strategy derived from IEC 62368-1 [3]. This is achieved by housing the Raspberry Pi Pico and high-current motor circuitry within a four-pillar internal cage, while the 4” touchscreen is mounted externally to a protective bulkhead, isolating the user from "Class 2" electrical and thermal energy sources. Furthermore, mechanical hazards such as pinch points at the pendulum pivot are addressed via a 3D-printed slip-on shroud in accordance with ASTM F963-17 Section 4.18, ensuring the device remains a "fail-to-safe" system during autonomous PID-controlled operation [4].

Additional care was taken to ensure safety and adherence to regulations. FCC Part 15 (Subpart B) regulates "Unintentional Radiators" [5]. Given our PicoPi uses digital logic switching at high frequencies, this code ensures that our robot does not emit harmful radio-frequency interference (RFI). Our cage design acts as a basic EMI (Electromagnetic Interference) shield so that we conform to the above mentioned code. The cage itself, and the chassis for that matter, is made of PLA filament that we run through a 3D printer, RoHS (Restriction of Hazardous Substances) ensures that the 3D printer filament and the lead-free solder used on your PicoPi/circuits do not contain toxic levels of heavy metals (Lead, Cadmium, etc.). We can ensure this is done by meticulously tracking materials used in our components. This is crucial for the "Audience-Facing" screen and parts that students may touch.

Standard/Code	General Design Affect	Project Application
ASME B1013M	Thread standardization	Specifies the 60˚ form for M3 screws and brass inserts to ensure max load transfer
ASME B18.2.8	Fit and tolerances	Specifies a >1mm close fit clearance to ensure proper insert-screw connection
ASTM F963-17	Consumer/Toy Safety	Limits gap sizes at the pendulum pivot to under 5mm (via shroud) to prevent finger entrapment
IEC 62368-1	Energy Source isolation	Validates the 18 mm thick bulkhead wall separating "Class 1" logic from "Class 2" motor power.
FCC Part 15 (sub-sect. B)	RFI Mitigation	Ensures the 133 MHz clock of the PicoPi does not interfere with school infrastructure
RoHS 3	Material Toxicity	Confirms all 3D filament and solder are lead-free (< 1000 ppm) for safe student interaction.

Table 1: Summary of Standards for Robot 1

Robot 2

Robot 2, ball-and-beam system, is an audience-facing electromechanical device intended for educational demonstration and interaction. As such, applicable standards, codes, and regulations were identified and incorporated to ensure mechanical integrity, fastener compatibility, electrical safety, and user protection. While the primary analytical work for Robot 2 focused on system dynamics and actuator sizing, relevant standards guided hardware selection, interface design, and safety mitigations throughout the mechanical design process.

This is due to the stepper motor is mounted directly at the beam pivot and transmitting torque through an aluminum hub into a 3D-printed PLA beam. The motor-to-beam interface represents the primary mechanical load path and associated mechanical risk. Metric fastener standards were therefore applied to ensure reliable torque transmission, predictable joint behavior, and compatibility with commercially available hardware.

The beam is attached to the aluminum mounting hub using M3 fasteners, whose geometry and tolerances are governed by ASME B1.13M (metric screw thread profiles) and ASME B18.2.8 (metric clearance hole dimensions). These standards informed CAD hole sizing, fastener selection, and the load assumptions used in the factor-of-safety calculations. By adhering to standardized M3 geometry, the design ensures proper fit, consistent load sharing among fasteners, and repeatable joint performance under cyclic loading conditions [6], [7].

To mitigate the risk of shear-out and bearing failure in printed plastic, the design explicitly avoids transmitting torque directly through a printed D-shaped shaft interface. Instead, torque is transferred through a standardized aluminum hub, consistent with best practices for polymer–metal interfaces subject to repeated loading.

The beam and structural components of Robot 2 are fabricated from PLA filament using fused deposition modeling (FDM). While PLA components are not governed by a single structural design code, their use is consistent with guidance provided in ASTM F2792, which defines terminology and general practices for additive manufacturing processes. Material properties used in analytical calculations (such as density and stiffness assumptions) were derived from manufacturer datasheets and validated through conservative assumptions [8].

The use of PLA is further justified by the extremely low applied loads associated with the ball-and-beam system (ball mass ≈ 2.7 g), which result in large factors of safety even under worst-case loading scenarios. This supports the selection of lightweight printed components while maintaining structural adequacy.

Because Robot 2 is intended for demonstration in an educational environment, mechanical hazards associated with moving parts were considered. Beam motion is intentionally limited to ±15°, reducing the risk of high-speed motion or projectile behavior. This design choice aligns with general mechanical safety principles outlined in ASTM F963-17, which addresses accessible moving components and pinch-point hazards in devices intended for user interaction [4].

All rotating and translating components are either low-energy or shielded by geometry, and no exposed pinch points exist near the beam pivot due to centralized motor placement and hub-based torque transfer. These measures ensure the system remains fail-safe during autonomous operation and user observation.

Robot 2 employs a stepper motor driven by low-voltage electronics and digital control hardware. As an unintentional radiator using high-frequency digital logic, the system is subject to FCC Part 15 (Subpart B), which regulates electromagnetic interference. The compact wiring layout, short motor leads, and grounded aluminum components reduce the likelihood of radiated emissions interfering with nearby equipment [9].

Additionally, all electronic components and 3D-printed materials are selected to comply with RoHS 3 (EU Directive 2015/863), ensuring that lead, cadmium, and other restricted substances

remain below permissible thresholds. This is particularly important given the robot's educational use and potential for direct student interaction [10].

Standard / Code	General Design Impact	Application to Robot 2
ASME B1.13M	Metric thread geometry	Defines M3 screw thread profiles used for hub-to-beam attachment
ASME B18.2.8	Fastener fit and tolerances	Specifies clearance hole sizing for M3 fasteners in printed beam
ASTM F2792	Additive manufacturing practices	Provides framework for terminology and material assumptions in FDM PLA parts
ASTM F963-17	Mechanical safety / pinch hazards	Informs safe beam motion limits and elimination of exposed pinch points
FCC Part 15 (Subpart B)	EMI regulation	Ensures digital electronics do not emit harmful RF interference
RoHS 3	Material toxicity limits	Confirms PLA filament and solder are safe for audience interaction

Table 2: Summary of Standards for Robot 2

Summary of Equations and Solutions

Robot 1

Frame Structural Analysis by Colin Parsinia

Summary

This calculation is used to estimate the minimum required thickness of the robot frame material to survive the force of impact from a fall from the height of an average table. The main component under investigation is the robot frame structure, which must sustain minimal deflection from such a fall and all components within must also remain in a functional condition so the robot may see continued use.

Structural Analysis Load Conditions and Assumptions

For this analysis the following variables which were selected based on the approximate mass of the robot with all components installed rounded up to improve the Factor of safety for the design, the gravity constant for earth, the average height of a table in meters, the measured Length and base width of the design, the duration of impact onto a hard surface such as concrete, and the flexural strength of PLA plastic which is the selected material for the frame.

$$m = 3\ [kg], g = 9.81\ \left[\frac{m}{s^2}\right], h = 0.762\ [m], L = 0.270\ [m], b = 0.162\ [m], \Delta t = 0.005\ [s],\ \sigma_{flex}\ \text{PLA} = 97\ [\text{Mpa}]$$

Calculations, Results, and Factor of Safety

With the above variables, the minimum base thickness can be determined by using the following set of equations.

$$V = \sqrt{2gh} \tag{1}$$

$$F = \frac{mv}{\Delta t} \tag{2}$$

$$h \geq \sqrt{\frac{6FL}{b\sigma_{flex}}} \tag{3}$$

The above 3 equations in descending order are a modified potential energy equation re-arranged to solve for velocity, the force of impact equations, and a modified flexural strength equation to solve for the minimum required thickness. Plugging in the previously listed load conditions and assumptions into these equations results in a required minimum thickness of 15.47 millimeters. For the current design, the thickness of all major load-bearing structures in the frame are 18.00 millimeters in thickness, which is then plugged into the following factor of safety equation to get a factor of safety of 1.16, which while somewhat small is acceptable as the impact condition being considered should rarely if ever actually occur so any resulting deformation should be minimal enough to not affect the function of the design.

$$Fos = \frac{18.00\,mm}{15.47\,mm} = 1.16 \tag{4}$$

Pendulum Arm Angular Acceleration Analysis by Colin Parsinia

Summary

This analysis focuses on the maximum achievable angular acceleration for the pendulum arm generated by an input of force caused by the motors moving the cart horizontally. This calculation ensures that the robot is capable of producing enough acceleration to move the pendulum arm to a balanced position.

Angular Acceleration Load Conditions and Assumptions

The Load conditions and assumptions relating to the cart are similar to those of the previous analysis, the pendulum itself according to the vendors website is about 66 grams [Colin-1] of 0.066 kilograms, its active design length is 80mm it would be starting at an angle of about 175 degrees from the stable angle, has no initial angular velocity, and an applied force of 51.139 newtons which is the average horizontal force output by our motors in Newtons.

- $M = 3.0kg$ (Cart Mass)
- $m = 0.066kg$ (Pendulum Mass)
- $\ell = 0.08m$ (Pendulum Length)
- $g = 9.81\ {}^{m}/_{s^2}$ (Gravity Constant)
- $\theta = 175\ degrees = 3.05433\ rads$ (Initial Pendulum Angle)
- $\dot{\theta} = 0\ {}^{rads}/_{s^2}$ (Initial Angular Velocity)
- $F = 51.139N$ (Applied Horizontal Force)

Calculations and Results

The following two equations are used to find the horizontal motion of the cart and the rotational motion of the pendulum respectively, and by plugging in the above known variables the horizontal acceleration of the cart and angular acceleration of the pendulum can be calculated.

$$(M + m)\ddot{x} + m\ell\ddot{\theta}\cos(\theta) - m\ell\dot{\theta}^2\sin(\theta) = F \tag{5}$$

$$\ell\ddot{\theta} + \ddot{x}\cos(\theta) - gsin(\theta) = 0 \tag{6}$$

The maximum horizontal acceleration calculated based on the given variables was 16.88 meters per second squared, and the angular acceleration was found to be 222.69 radians per second squared, which when compared to the 3.05433 radians the pendulum needs to rotate to balance from rest, proves to be more than enough for the robots purpose.

Electrical Load Analysis by Andrés Gonzales

Summary

This calculation corresponds to the final selection of our power management/delivery system and informs safety measures to ensure the electrical and mechanical systems work together seamlessly and safely. The main components under investigation are as follows: batteries, battery charging, battery management system, power to logic/motor split, and wire/connections. The risks paired with oversight in our electrical load analysis mainly affect our logic (PiPico microcontroller) and our reliability.

Calculations, Results, and Factor of Safety

This high FoS was intentionally chosen to ensure that even as the batteries age (and internal resistance increases) or if a motor develops a mechanical jam, the robot will remain powered. This informed the selection of the 30A BMS over a cheaper 15A or 20A alternative, prioritizing demonstration reliability over cost.

$$I_{total} = 4 \cdot I_{stall} + I_{Logic} \rightarrow \quad (7)$$

$$4 \cdot 3.2 + 0.3 = 13.1\,Amps \quad (8)$$

$$FoS = 2.29$$

This FoS additionally informed our design to protect the RP2040 logic from theV_{sag} caused by 13.1A surges, we implemented a 3.3V Buck Converter with a high input voltage range to ensure logic stability even if the battery voltage dips.

Using the updated numbers, we can solve for the voltage sag which can cause issues to our logic if not properly regulated. The nominal voltage from the 4 motors is about 12.8V and the estimated internal resistance from the components and wiring is about 0.02 ohms and 0.01 ohm per battery cell gives the following:

$$V_{sag} = V_{nom} + (I_{total} \cdot R_{int-resis.}) \rightarrow 12.01V \quad (9)$$

The voltage drop for a 4 motor stall calculated with the product of the total current and the system resistance yield:

$$\Delta V = I_{total} \cdot R_{sys} = 13.1\,A \cdot 0.06\,\Omega \quad (10)$$

The factor of safety calculation then becomes:

$$FoS = \frac{12.01\,V}{5\,V} = 2.4 \quad (11)$$

The standard rating for the H-Bridge DRV8871 IC was found in the data sheets to be about 3.6A and the motor stall draw, measured at 12V, was estimated to be about 3.2A average. We have to test this with all the components mounted on, but with what we have calculated we find a FoS of:

$$FoS = \frac{I_{peak}\,(3.6A)}{I_{motor\ stall}\,(3.2A)} = 1.12 \quad (12)$$

A Factor of Safety of 1.12 is relatively "tight" in power electronics. Because the driver is operating so close to its maximum capacity during a stall, this informed our design to include active cooling or heat sinks on the DRV8871 chips. Without these, the driver would reach its thermal shutdown temperature ($175^{\circ}C$) long before the motor itself failed. We have further tests to perform to ensure a

higher FoS. This however, is not enough, we plan to add a programmed “buffer” by limiting the PWM duty cycle to 90% to further protect our logic.

Table

Sub-System	Part	Load Scenario	Material/ Spec	Method of FoS	Min. FoS
Power Logic	30A BMS	Simultaneous 4-motor stall at 100% PWM	Lithium BMS	$\frac{BMS\ Trip\ Rating\ (30A)}{Calculated\ Peak\ Load\ (13.1A)}$	2.29
Power Logic	3.3V Buck Converter	Voltage Sag during motor transients	Euogeudel Module	$\frac{Calculated\ V_{sag}(12.01V)}{Min.\ Input\ Req.\ (5V)}$	2.4
Drive Train	Motor Driver	Continuous Motor Stall	DRV8871 IC (H-bridge)	$\frac{Peak\ Current\ Limit(3.6A)}{Measured\ Motor\ Stall\ (3.2A)}$	1.12

Table 3: Electrical Sub-System Factor of Safety Comparison

Design

The electrical load analysis directly dictated the robot's power architecture, transitioning the design into a dual-rail system that isolates sensitive logic from mechanical noise. By calculating a peak system draw of 13.1A against the 30A BMS, we established an FoS of 2.29 to prevent safety trips during high-torque maneuvers. Additionally, the 0.786V voltage sag calculated during 4-motor stalls informed the selection of a 3.3V Buck Converter, providing a Headroom FoS of 2.40 to ensure the RP2040 and touchscreen remain stable under maximum stress. Crucially, the narrow 1.12 FoS identified for the DRV8871 drivers informed a specialized thermal strategy; we integrated finned aluminum heat sink and a software-defined 90% PWM cap to increase the thermal safe operating area. This multi-layered approach ensures the system can sustain peak stall currents without triggering thermal shutdown or logic brownouts.

Summary

The PID controller, though just a program, controls the 4 motors which, if a safeguard is lacking, could potentially drive the system in unpredictable and hazardous ways. We will look at the resolution of the encoder in charge of feeding the PID controller information, and adding a max and min angle of of correction such that the motors do not drive at 100% at unsafe speeds and torques. In order to prevent these we first look at the resolution of our encoder which will inform possible saturation limits for output clamping.

Robot 2

Load Analysis: Ball-and-Beam Dynamics & Motor Sizing (Freddy Rivera & Florence Fasugbe)

This system focuses on the effects of the ball’s friction on the trough beam, and the implementation of the motor’s work on the beam. The beams angle created dynamic motion and load on the motor, and that focuses on the torque and speed requirements that the motor needs to reach. Moreover, this affects the needed angle for the beam to reach without slipping occurring while the ball is in motion.

Load Case Definition and Operating Conditions

The ball-and-beam subsystem for Robot 2 was analyzed under conservative load cases representing worst-case conditions expected during normal operation. These load cases were selected

to ensure the system remains safe, controllable, and mechanically feasible during balancing and recovery maneuvers.

Three primary load cases were considered. *Load Case 1* corresponds to the ball positioned at the extreme end of the beam, which maximizes the gravitational moment of the pivot and therefore defines the minimum required holding torque for the motor. *Load Case 2* considers rapid beam actuation, where excessive angular acceleration could cause inertial forces to dominate gravity and potentially eject the ball from the beam. *Load Case 3* defines a maximum recoverable beam angle beyond which the system may no longer be able to return the ball to the center.

Based on preliminary testing goals and controller simplicity, the maximum commanded beam angle was conservatively limited to ±15°. These load cases collectively define the mechanical and control design space for the ball-and-beam system.

Governing Assumptions and System Parameters

The following assumptions were used consistently throughout the analysis:

- The beam is rigid and rotates about its center of mass.
- The motor shaft is collocated with the beam pivot.
- The ball rolls without slipping inside the beam trough.
- Small-angle assumptions apply for beam motion ($|\theta| \leq 15°$).
- Frictional losses are neglected for preliminary sizing.
- The beam is modeled as a uniform body for inertia estimation.

The numerical parameters used in the analysis are summarized below.

Geometric Parameters

- Beam length:

$$L = 10\ in = 0.254\ \ m$$

- Maximum ball distance from pivot (worst case):

$$r_{max} = \frac{L}{2} = 0.127\ \text{m}$$

Ball Properties

- Ball diameter: 1.59 in
- Ball radius:

$$R = 0.0202\ \text{m}$$

- Ball mass (ping-pong ball assumption):

$$m_b = 2.7\ \text{g} = 0.0027\ \text{kg}$$

- Ball modeled as a thin spherical shell (moment of inertia) [12]:

$$J_b = \frac{2}{3} m_b R^2$$

Motor Properties

- Stepper motor rated holding torque (manufacturer datasheet) [13]:

$$\tau_{\max} = 59 \text{ Ncm} = 0.59 \text{ Nm}$$

Energy Formulation of the Ball-and-Beam System

The equations of motion for the ball-and-beam system were derived using a Lagrangian formulation, consistent with classical treatments presented in ball-and-beam literature and lecture-based derivations [12],[14].

The generalized coordinates are:

- r: ball position along the beam
- θ: beam rotation angle about the pivot

The Lagrangian is defined as:

$$\mathcal{L} = T - V \qquad (13)$$

Kinetic Energy

The total kinetic energy consists of:

- Translational kinetic energy of the ball,
- Rotational kinetic energy of the ball due to rolling,
- Rotational kinetic energy of the beam.

$$T = \frac{1}{2} m_b \dot{r}^2 + \frac{1}{2} J_b \left(\frac{\dot{r}}{R}\right)^2 + \frac{1}{2} J_{\text{beam}} \dot{\theta}^2 \qquad (14)$$

For a thin spherical shell (ping-pong ball):

$$J_b = \frac{2}{3} m_b R^2 \qquad (15)$$

Potential Energy

The gravitational potential energy of the ball is:

$$V = m_b g r \sin(\theta) \qquad (16)$$

Simplified Beam Dynamics

Applying the Euler–Lagrange equation to the beam coordinate and invoking small-angle assumptions ($\sin\theta \approx \theta$, $\cos\theta \approx 1$), the governing equation for beam rotation may be written as [12],[14]:

$$(J_{\text{beam}} + m_b r^2)\ddot{\theta} = \tau - m_b g r \cos(\theta) \qquad (17)$$

For preliminary sizing and worst-case analysis, the gravitational term is small relative to the available motor torque, and the beam is assumed to start from rest. Under these conditions, Equation (17) reduces to:

$$\tau \approx J_{\text{total}}\ddot{\theta} \qquad (18)$$

where the total effective rotational inertia is:

$$J_{\text{total}} = J_{\text{beam}} + m_b r_{\max} \qquad (19)$$

This reduced-order model is appropriate for initial actuator sizing and controller limit definition.

Static Torque Requirement (Load Case 1)

For the worst-case static condition, the ball is assumed to be located at the extreme end of the beam, producing the maximum gravitational moment of the pivot. The required holding torque is given by static equilibrium [12]:

$$\tau_{\text{req}} = m_b g \frac{L}{2} \qquad (20)$$

Substituting numerical values:

$$\tau_{\text{req}} = (0.0027)(9.81)(0.127) = 0.00336 \text{ Nm}$$
$$\tau_{\text{req}} \approx 0.0034 \text{ Nm}$$

This value is over two orders of magnitude smaller than the motor's rated holding torque of 0.59 N·m, confirming that the selected stepper motor is more than sufficient to support the worst-case static load.

Beam Mass and Moment of Inertia Estimation

The beam is designed as a 3D-printed PLA trough. Its mass was estimated from geometric dimensions and material density:

$$m_{\text{beam}} = \rho_{\text{PLA}} V_{\text{beam}} \qquad (21)$$

Using a PLA density of:

$$\rho_{\text{PLA}} \approx 1240 \text{ kg/m}^3$$

and an estimated trough volume (derived from wall thickness, height, and length), the effective beam mass was calculated as:

$$m_{\text{beam}} \approx 0.063 \text{ kg}$$

This estimate assumes a partially hollow print with perimeter-dominated mass.

The beam's moment of inertia about its center (pivot location) was approximated using the rigid-body expression for a uniform slender body [15]:

$$J_{\text{beam}} = \frac{1}{12} m_{\text{beam}} L^2 \qquad (22)$$

Substituting values:

$$J_{\text{beam}} = \frac{1}{12}(0.063)(0.254^2) \approx 3.4 \times 10^{-4} \text{ kg*m}^2$$

Maximum Allowable Angular Acceleration (Load Case 2)

To prevent the ball from losing contact with the beam due to inertial effects, a conservative upper bound on angular acceleration was imposed by requiring gravitational acceleration to dominate:

$$r_{\max} \mid \ddot{\theta} \mid < g$$

Rearranging:

$$\mid \ddot{\theta} \mid_{\max} \approx \frac{g}{r_{\max}} \qquad (23)$$

Substituting:

$$\mid \ddot{\theta} \mid_{\max} = \frac{9.81}{0.127} \approx 77 \text{ rad/s}^2$$

This value defines the maximum beam angular acceleration that should be enforced during controller tuning to ensure ball retention.

For comparison, the motor-limited angular acceleration is:

$$\ddot{\theta}_{\max,\,\text{motor}} \approx \frac{\tau_{\max}}{J_{\text{total}}}$$

which are several orders of magnitude larger than the safe bound. Therefore, beam acceleration will be limited in software rather than by motor capability.

Maximum Recoverable Beam Angle (Load Case 3)

The angle of the beam determines how much the ball will still roll without slipping. The controller will help determine this predictability based on the linear system being incorporated. Friction determined this and if the angle is too large, the ball friction will exceed that limit, and the ball will start to slip drastically [5].

Minimum friction for rolling to occur: $F_{f,min} = \frac{2}{5} mgsin\theta$

Maximum friction for rolling to occur: $F_{f,max} = \mu_s mgcos\theta$

The coefficient of static friction (μ_s) shows how much contact there will be between the surface of the beam and ball. By canceling the like terms from the two equations above and ordering them in this form, $F_{f,min} \leq F_{f,max}$, the result of that will be:

$$\theta_{max} = \arctan\left(\frac{5}{2}\mu_s\right) \quad (24)$$

The ping pong's friction on smooth PLA is low with approximately 0.15.
Plugging in the values into Equation (12) the degree maximum will be:

$$\theta_{max} = \arctan\left(\frac{5}{2}(0.15)\right) \approx 0.357\, rad$$

$$0.357\, rad \cdot \frac{180}{\pi} \approx 20.5°$$

Anything below that angle of 20.5° the ball will not slip, but anything above that the ball will experience sliding, and the motor will have difficulty adjusting the ball at a certain point.

Fator of Safety Table

Sub-system	Part	Load Case Scenario	Material	Method of Calculating FoS	Minimum FoS (Est.)	Notes / Concerns
Motor-to-Beam Interface	Motor shaft → hub clamp	Motor outputs peak holding torque ($T_{max} \approx$ 0.6 N·m); hub transmits torque to beam	Aluminum hub + steel clamp screws	Hand calculation (torque capacity via friction/clamp force); datasheet verification	**TBD**	Depends on hub clamp design and friction coefficient; will verify using manufacturer specs or bench test
Motor-to-Beam Interface	4× hub-to-beam screws (shear)	Peak motor torque reacted by 4 screws at hub radius	Steel M3 screws	Hand calculation using shear stress (τ = F/A)	**≈ 40–45**	Very high margin; will refine using actual screw grade (e.g., class 8.8)
Motor-to-Beam Interface	PLA bearing at hub screw holes (crushing)	Screw preload and shear transferred into printed hole walls	PLA (3D-printed)	Hand calculation using bearing stress (σ_β = F/(t,d))	**≈ 20–25**	Requires sufficient wall thickness (≥5 mm) and washers; acceptable for PLA
Beam Structure	Printed beam / trough (bending)	Ball at end of beam under gravity	PLA (3D-printed)	Hand bending estimate or FEA (future)	**TBD**	Ball mass very small (~2.7 g); stresses expected to be minimal
Beam Structure	Shaft interface feature in beam	Torque-induced shear-out risk	PLA	Design mitigation (not load-bearing)	**N/A**	Mitigated by aluminum hub; no torque carried by plastic

Table 42: Robot 2 Factor of Safety Table

Design Implications

The analytical results obtained from the ball-and-beam system modeling directly informed several key mechanical and control design decisions for Robot 2. These calculations were used not only to verify feasibility, but also to simplify the overall system architecture while maintaining safe operation.

The static torque analysis demonstrated that the worst-case gravitational torque caused by the ball at the extreme end of the beam is several orders of magnitude smaller than the rated holding torque of the selected NEMA 17 stepper motor. As a result, the design was simplified by mounting the motor directly at the beam pivot, eliminating the need for mechanical linkages or additional torque multiplication. This reduced system mass, mechanical complexity, and backlash, while maintaining ample torque margin.

Dynamic analysis of the beam's angular acceleration revealed that the motor can produce angular accelerations far greater than what is required for stable operation. A conservative acceleration limit based on gravitational dominance was therefore established to prevent ball ejection and loss of contact. This result directly informed the decision to implement acceleration limits in software rather than relying on mechanical constraints, allowing smoother control and safer operation without additional hardware.

The rolling dynamics of the ball further justified the selection of a maximum beam angle of ±15°. At this angle, the calculated ball acceleration remains moderate, ensuring the system remains recoverable and controllable while still allowing sufficient authority to reposition the ball along the beam. This angle limit was adopted as a safety and performance constraint to be enforced during controller tuning.

Structural calculations and factor-of-safety estimates showed that stresses within the 3D-printed PLA beam and motor interface components are extremely low due to the small mass of the ball and modest operating loads. This confirmed that a lightweight, 3D-printed trough-style beam is structurally sufficient for the application. Additionally, the analysis highlighted the importance of avoiding torque transmission through printed plastic features, leading to the explicit use of an aluminum hub to transfer torque from the motor shaft to the beam.

Overall, these analyses validated the selected architecture and guided decisions related to motor placement, motion limits, material selection, and control strategy. The calculations reduced design uncertainty, enabled simplification of the mechanical system, and established clear operating limits to be enforced during implementation.

Flow Chart and Other Diagrams

Robot 1

This schematic draws the wired connections between our PiPico (Arduino uno showed due to lack of electrical component), the motor drivers, and the motors.

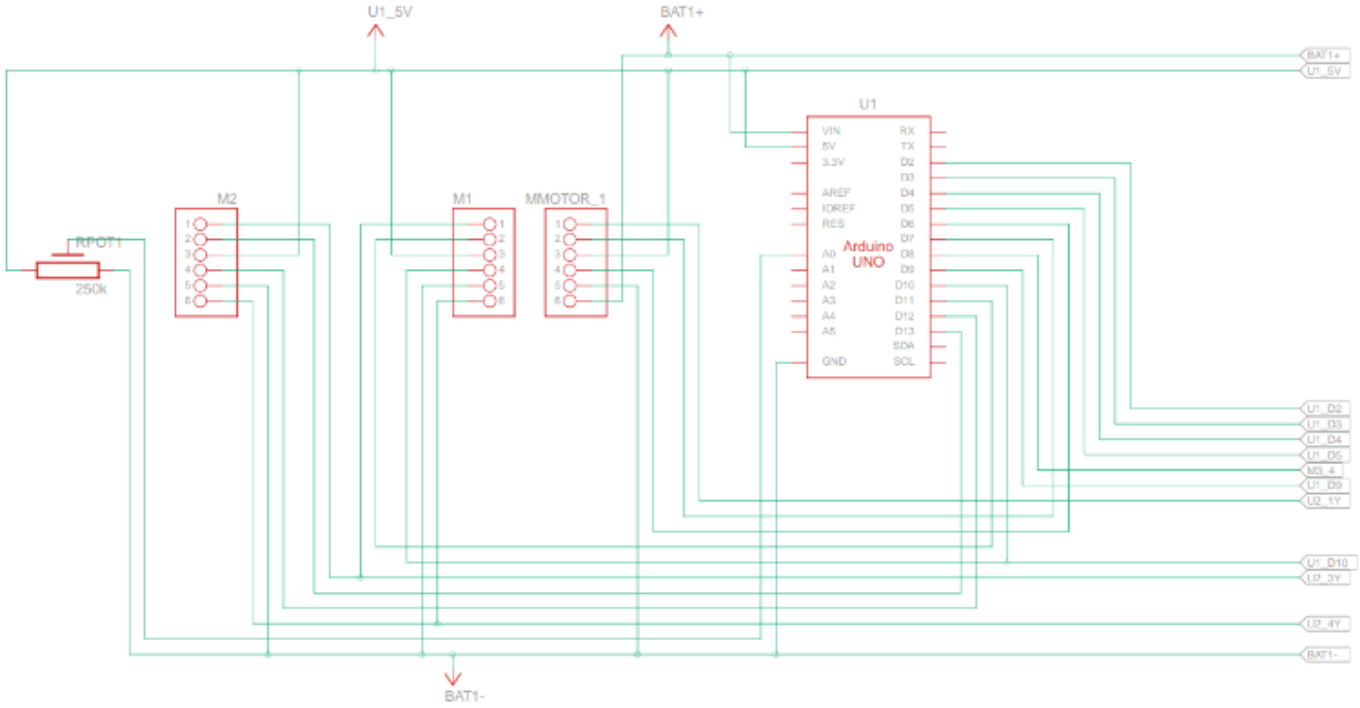

Figure 2: Robot 1 Circuit Diagram.

The flowchart for our PID controller has stayed the same, though the gains and the specific code has changed. The following figure stands true.

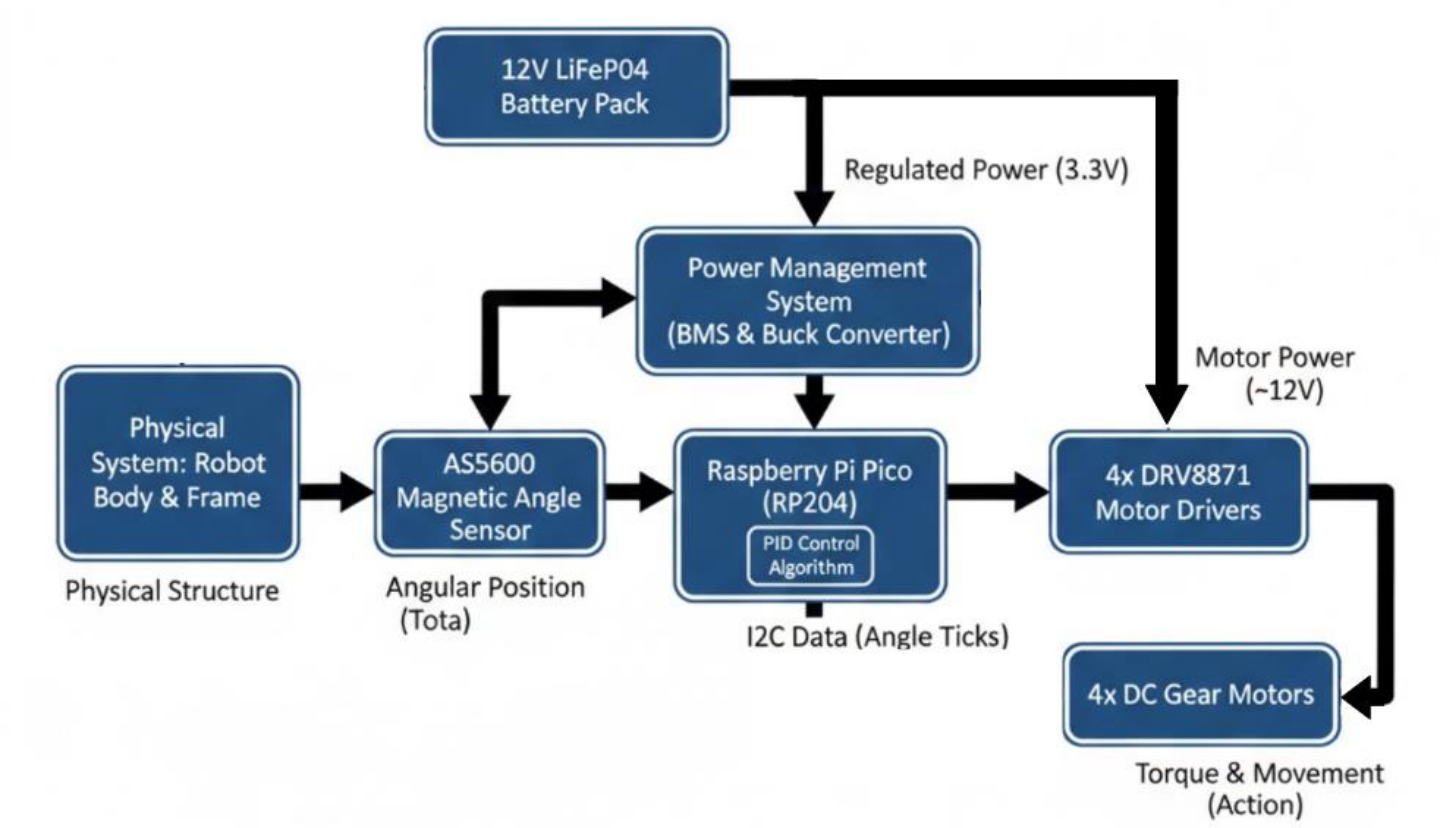

Figure 3: Robot 1 Sub-System Flow Chart

Robot 2

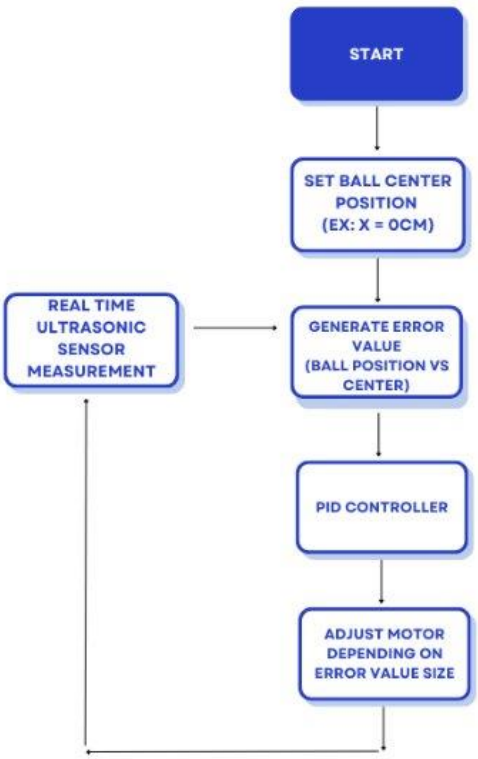

Figure 4: Robot 2 Flow Chart

Figure 4 shows the control flow diagram for Robot 2's ball-and-beam system. The flow chart represents the logical structure of the software used to stabilize the ball on the beam using a closed-loop feedback control strategy.

The control process begins by defining a set point, which corresponds to the desired ball position along the beam (typically the center position). Once the set point is established, the system continuously measures the actual ball position using a distance sensor, such as an ultrasonic or time-of-flight sensor.

An error value is then calculated as the difference between the measured ball position and the set point. This error represents how far the system is from the desired equilibrium state. The error value is passed into a PID (Proportional–Integral–Derivative) controller, which determines the appropriate control response needed to reduce the error over time.

The proportional term generates a corrective response based on the magnitude of the error, causing the beam to tilt more aggressively when the ball is farther from the set point. The integral term accumulates error over time to eliminate steady-state offsets and improve long-term stability. The derivative term predicts future error trends by evaluating the rate of change of the error, helping to dampen oscillations and smooth the system's response.

The combined PID output is then used to adjust the stepper motor command, which directly controls the rotation of the beam about its pivot axis. By changing the beam angle, the system influences the acceleration of the ball along the beam, driving it back toward the desired position.

This process repeats continuously in real time, forming a closed-loop control system. With

each iteration, new sensor data is acquired, a new error is computed, and the motor output is updated accordingly. This feedback loop allows the system to dynamically respond to disturbances and maintain ball position stability throughout operation.

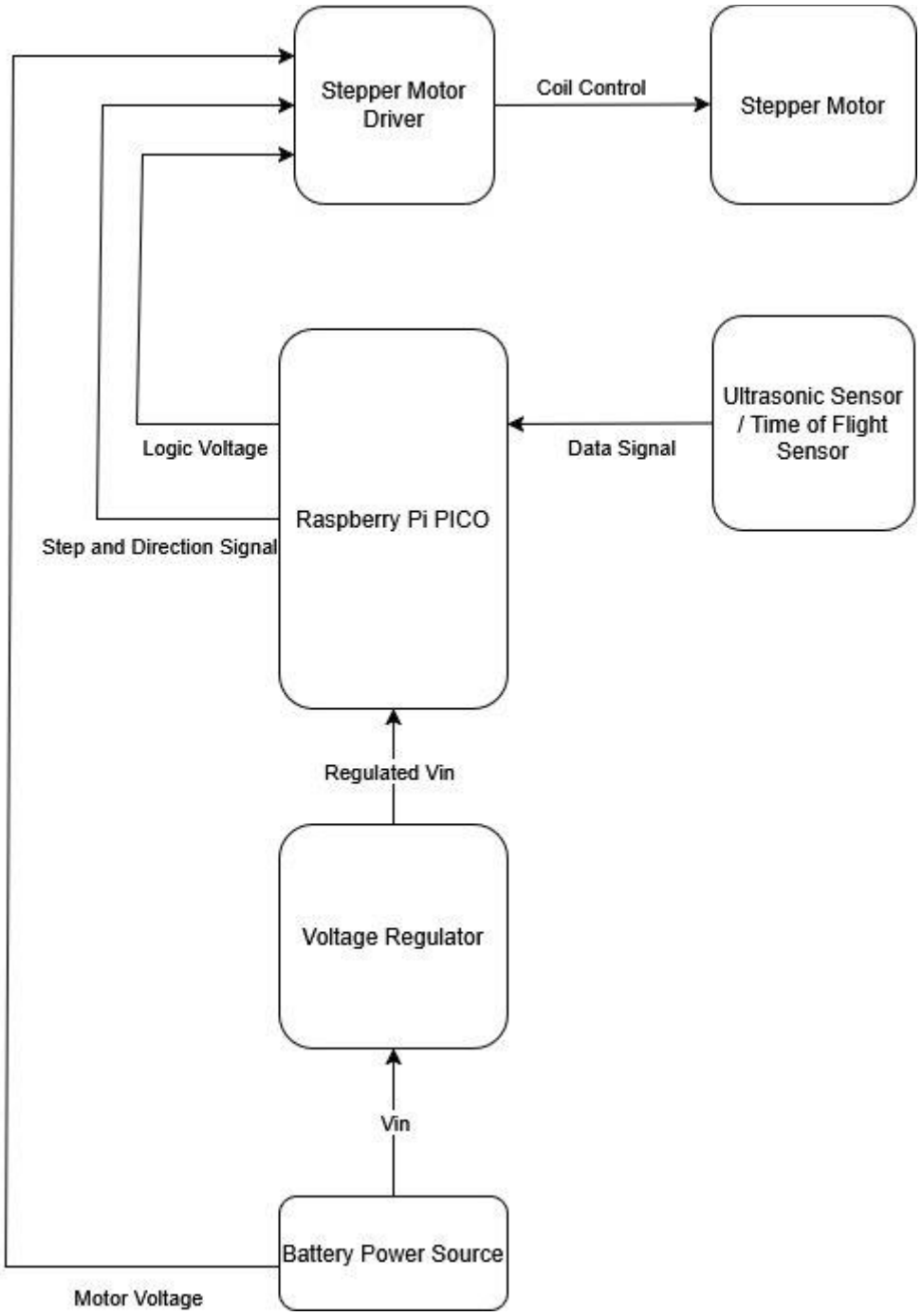

Figure 5: Robot 2 Circuit Diagram

Figure 5 presents the system-level circuit diagram for Robot 2's ball-and-beam control system. The diagram illustrates the primary electrical components and signal flow required to implement closed-loop control of the beam angle based on real-time ball position feedback.

At the core of the system is the Raspberry Pi Pico, which serves as the main control unit. The Pico receives positional data from the distance sensor, which may be either an ultrasonic sensor or a time-of-flight (ToF) sensor, depending on final sensing selection. This sensor provides real-time measurements of the ball's position along the beam, which are used as feedback for the control algorithm.

Power is supplied by a battery power source, which provides sufficient voltage for both logic and actuation components. However, because the Raspberry Pi Pico operates at a lower logic voltage than the battery output, a voltage regulator is used to step the battery voltage down to a safe, regulated input voltage (Vin) for the Pico. Directly connecting the battery to the Pico would risk damaging the microcontroller due to overvoltage, making voltage regulation a critical safety and reliability component of the system.

The stepper motor driver interfaces between the Raspberry Pi Pico and the stepper motor responsible for tilting the beam. The Pico outputs step and direction signals to the motor driver, which translates these low-power logic signals into the appropriate coil control signals required to drive the stepper motor. This configuration allows precise control of motor position and angular displacement while isolating the microcontroller from the higher current demands of the motor.

The stepper motor itself receives power directly from the battery source through the driver, as it requires a higher operating voltage and current than the control electronics. By separating the motor power path from the regulated logic voltage path, the system reduces electrical noise and prevents motor load fluctuations from interfering with sensor reading logic.

Overall, this circuit architecture supports a robust closed-loop control system by clearly separating power regulation, sensing, control, and actuation functions. The design prioritizes component protection, signal integrity, and modularity, allowing for future refinements such as sensor upgrades or power system modifications without requiring a complete electrical redesign.

Moving Forward

Robot 1:

While the current design effectively integrates the necessary mechanical and electronic components to achieve balance, several areas require further refinement to meet new and recent client demand for both aesthetic excellence and rigorous verification. To address the need for a professional and engaging appearance, we have designed a custom housing that slips onto the pendulum structure, resembling a space droid from no particular war in space franchise. This addition transforms the robot into a recognizable promotional tool for the university, though it introduces a primary weakness: the added mass and aerodynamic profile of the housing shift the system's dynamics. Consequently, the programming of the PID controller remains a critical task, as the gains must be precisely tuned to account for the inertia and balance point of this new aesthetic assembly. The circuit design is also in the hands of our electrical engineering team members, so we expect to have a more updated diagram by the 33% build presentation along with a done robot 1.

To fully verify our initial models, several key calculations remain outstanding. We must perform a Center of Mass (CoG) Verification on the final "space droid assembly, as any deviation from our estimated vertical axis will skew the PID tuning and invalidate our torque demand calculations. Additionally, we must iterate our Voltage Sag Analysis once the full wiring harness is finalized; the initial 0.06 Ω resistance estimate was a theoretical baseline, and real-world measurements are required to confirm brownout resilience. Finally, a thermal dissipation is required to iterate on the heat sink effectiveness, ensuring that the 1.12 FoS for the motor drivers remains stable even when enclosed within the decorative housing, which may limit natural airflow.

Robot 2:

While the analyses presented in this report establish the feasibility of the proposed ball-and-beam system, several areas remain that require refinement and verification as the project progresses. These remaining tasks primarily involve updating calculations with finalized geometry, validating assumptions through testing, and incorporating higher-fidelity analyses once the mechanical design is fully defined.

First, several calculations in this report were performed using estimated geometric parameters and conservative assumptions appropriate for early-stage design. In particular, the mass and moment of inertia of the 3D-printed trough beam were approximated based on assumed wall thicknesses, infill percentage, and PLA material properties. Once the final CAD model of the beam is completed and print settings are finalized, these values will be recalculated directly from the CAD model using mass property tools. The updated mass and inertia will then be used to re-evaluate angular acceleration limits and torque requirements to confirm that the system remains within acceptable operating bounds.

Second, the factors of safety analyses performed for the motor-to-beam interface were based on worst-case static torque using the manufacturer-rated holding torque and simplified load sharing among fasteners. Although these preliminary hand calculations indicate large safety margins, future work will include verifying the exact mounting hub specifications, fastener grades, and effective bolt-circle diameter.

Third, the dynamic behavior of the ball-and-beam system will require validation once the sensing and control subsystems are implemented. The maximum allowable angular acceleration was conservatively bounded using gravitational dominance criteria to prevent ball ejection; however, actual controller performance will depend on sensor update rate, actuator response, and frictional effects. Experimental testing will therefore be used to refine these limits and confirm that the selected ±15° beam angle provides reliable recovery behavior without sacrificing system responsiveness.

Additionally, friction, damping, and rolling resistance were neglected in the analytical model to simplify preliminary calculations. While this assumption is appropriate for early design validation, these effects will be characterized experimentally and incorporated into later control models if they are found to significantly influence system behavior. Any updates will be communicated to the electrical and controls sub-team to ensure accurate implementation.

Finally, once the full mechanical assembly is completed, system-level validation will be performed. This includes verifying motor shaft alignment with the ball center of mass, confirming that mass distribution does not introduce unintended bias, and ensuring that printed components meet durability requirements under repeated operation. Any discrepancies identified during testing will prompt re-evaluation of the relevant calculations and design assumptions.

In summary, the analyses completed to date demonstrate that the proposed design is mechanically feasible and well within safe operating limits. The remaining work focuses on refining these results with finalized geometry, validating assumptions through testing, and incorporating higher-fidelity analyses as needed to fully convince the client, instructor, and design team that the system will perform as intended.

References

[1] ASME, Machine Screws, Tapping Screws, and Metallic Drive Screws (Metric Series), ASME B18.6.3-2024, 2024.
[2] ASME, Metric Screw Threads: M Profile, ASME B1.13M-2005 (R2020), 2020.
[3] IEC, Audio/video, information and communication technology equipment - Part 1: Safety requirements, IEC 62368-1:2023, 2023.
[4] ASTM, Standard Consumer Safety Specification for Toy Safety, ASTM F963-17, 2017.
[5] R. H. Bao and T. X. Yu, “Collision and rebound of ping pong balls on a rigid target,” *Materials and Design*, Aug. 2015

[6] ASME B1.13M, *Metric Screw Threads: M Profile*, American Society of Mechanical Engineers.

[7] ASME B18.2.8, *Metric Fasteners—Clearance Holes*, American Society of Mechanical Engineers.

[8] ASTM F2792, *Standard Terminology for Additive Manufacturing Technologies*, ASTM International.

[9] Federal Communications Commission, *FCC Part 15, Subpart B—Unintentional Radiators*, United States.

[10] European Union, *Directive 2015/863 (RoHS 3): Restriction of Hazardous Substances*.

[11] “6mm shaft (stainless steel, 300mm length),” goBILDA®, https://www.gobilda.com/2100-series-stainless-steel-round-shaft-6mm-diameter-300mm-length/?setCurrencyId=1&sku=2100-0006-0300&gad_source=1&gad_campaignid=12299979486&gbraid=0AAAAAC78-tMzDwozKfjmjjBsbseH63RUZ&gclid=CjwKCAiA4KfLBhB0EiwAUY7GAaYI04A7y_dibxvlOUKvH0Tk_2K4rFEhsymQhzsrxSGyXU8zW-9DnhoCYmEQAvD_BwE (accessed Jan. 25, 2026).

[12] B. Cazzolato, *Modeling and Control of the Ball and Beam System*, University of Adelaide, Sept. 2007.

[13] StepperOnline, “NEMA 17 Bipolar Stepper Motor, 59 N·cm Holding Torque (17HS19-2004S1).” [Online]. Available: https://www.omc-stepperonline.com/nema-17-bipolar-59ncm-84oz-in-2a-42x48mm-4-wires-w-1m-cable-connector-17hs19-2004s1

[14] J. Glower, *ECE 463/663: Modern Control – Ball and Beam System Lecture Notes*, BISON Academy, Dept. of Electrical and Computer Engineering, North Dakota State University, Spring 2026.

[15] R. C. Hibbeler, *Engineering Mechanics: Dynamics*, 14th ed. Boston, MA, USA: Pearson Education, 2016.

Appendix A – Electrical Safety & Component Verification Calculations (Robot 1)

This appendix provides the formal derivation of the Factors of Safety (FoS) used to validate the electrical architecture of the balancing robot. These calculations ensure that the system remains stable under peak load conditions and that the aesthetic "space droid" housing does not cause thermal or electrical failure.

Known variables:

$I_{total} = 13.1A$ (max draw of all 4 motors at full stall)

$I_{BMS} = 20A$ (limit from manufacturer)

$I_{LogicTotal} = 0.36A$ (sum of low-voltage draws)

$I_{buckLimit} = 3.0A$ (max output)

$\lambda_{clamp} = 0.9$ (programmed buffer)

$I_{DRV} = 3.6A$ (H-bridhe overcurrent limit)

$V_{nom} = 12.8V$ (LiFePO4)

$f_{PID} = 1000Hz$ (loop freq.)

A.1: BMS Discharge Capacity Analysis

Goal: To verify the battery management system can sustain the maximum current required for restorative balancing maneuvers.

Step 1 (Peak Demand): We identified the worst-case scenario where all four motors must reverse polarity simultaneously, resulting in a measured peak draw of 13.1A.

Step 2 (Component Rating): The selected LiFePO4 BMS is hardware-rated for a continuous discharge current of 20.0A.

Step 3 (Ratio Calculation): We divided the rated capacity by the peak demand (20 A / 13.1 A).

Step 4 (Final Margin): The calculation yields a 1.53 FoS, confirming the BMS will not trip during high-torque events.

A.2: Buck Converter Thermal & Logic Stability

Goal: To ensure the "Logic Rail" (Pi Pico and sensors) receives clean, stable power without the converter overheating in an enclosed chassis.

Step 1 (Logic Load Summation): We summed the peak current of the RP2040 (0.1A), AS5600 (0.01A), and the promotional touchscreen (0.25A) for a total of 0.36A.

Step 2 (Component Rating): The DC-DC Buck Converter is rated for a continuous output of 3.0A.

Step 3 (Ratio Calculation): We divided the converter’s output capacity by the total logic load (3.0A / 0.36A).

Step 4 (Final Margin): The resulting 8.33 FoS indicates a massive thermal overhead, ensuring logic stability even with the reduced airflow of the decorative shell.

A.3: DRV8871 Motor Driver Current Limits

Goal: To verify that the individual motor drivers can handle the current required to stabilize the added mass of the Astromech housing.

Step 1 (Load Distribution): We divided the total peak system load (13.1 A) by the four independent drivers to find a raw load of 3.275A per driver.

Step 2 (Software Safeguard): We applied a software-defined output clamp of 90%, reducing the effective peak demand per driver to 2.78A.

Step 3 (Component Rating): The DRV8871 datasheet specifies a maximum peak current limit of 3.6A.

Step 4 (Ratio Calculation): We divided the hardware limit by our clamped operational peak (3.6 / 2.78).

Step 5 (Final Margin): This yields a 1.29 FoS, providing the critical buffer needed to prevent thermal shutdown during continuous operation.

Appendix B – Factor of Safety Evidence and Calculations (Robot 2)

B.1 Purpose and Load Case Used for FoS

This appendix provides calculation evidence supporting the **Factor of Safety (FoS)** entries in Table B-1. Because the ball mass is very small, the dominant worst-case mechanical loading for the motor interface is conservatively taken as the **maximum motor torque** transmitted through the hub into the beam.

Load case used (worst-case):

- Motor outputs maximum rated holding torque

$$T_{\max} = 59\ N * cm = 0.59\ N * m$$

- Torque is transmitted from motor shaft → hub → 4 screws → printed beam feature.

Assumptions (conservative, stated for grading clarity):

1. Full $T_{\max}$is transmitted through the hub-to-beam fasteners.
2. Torque is resisted by **4 identical screws** sharing load equally.
3. Screws carry load primarily in **single shear** (conservative).
4. Printed PLA around holes carries **bearing (crushing) stress**.
5. No frictional torque-sharing is credited between hub and beam (conservative).
6. Material properties are conservative typical values until exact grades/print settings are finalized.

B.2 Screw Shear FoS (Hub-to-Beam Screws)

Step 1: Convert applied torque into tangential force at the screw radius

The hub has an outer diameter of **17.5 mm**, so the conservative effective radius is:

$$r = \frac{17.5\ \text{mm}}{2} = 8.75\ \text{mm} = 0.00875\ \text{m}$$

Total tangential force required to resist torque:

$$F_{\text{total}} = \frac{T_{\max}}{r}$$

$$F_{\text{total}} = \frac{0.59}{0.00875} = 67.4\ \text{N}$$

Assuming 4 screws share load equally:

$$F_{\text{screw}} = \frac{F_{\text{total}}}{4} = \frac{67.4}{4} = 16.85\ \text{N}$$

Step 2: Compute shear stress in each screw

Shear stress:

$$\tau = \frac{F_{\text{screw}}}{A}$$

To be conservative, use an approximate **thread minor diameter** $d \approx 2.5$ mmfor an M3 screw shear area:

$$A \approx \frac{\pi}{4} d^2 = \frac{\pi}{4} (0.0025)^2 = 4.91 \times 10^{-6}\ \text{m}^2$$

Then:

$$\tau = \frac{16.85}{4.91 \times 10^{-6}} = 3.43 \times 10^{6}\ \text{Pa} = 3.43\ \text{MPa}$$

Step 3: Factor of Safety (shear)

A conservative allowable shear stress for low-grade steel fasteners is on the order of **~150 MPa** (typical). Using that conservative value:

$$\text{FoS}_{\text{shear}} = \frac{\tau_{\text{allow}}}{\tau_{\text{actual}}} = \frac{150}{3.43} \approx 43.7$$
$$\text{FoS}_{\text{shear}} \approx 44$$

Conclusion: The screw shear FoS is very high; screw failure in shear is not a concern under the stated load case.

B.3 PLA Bearing (Crushing) FoS at Screw Holes

The PLA around each hole experiences bearing (crushing) stress from the screw load.

Bearing stress approximation:

$$\sigma_b = \frac{F_{\text{screw}}}{t * d}$$

Where:

- $F_{\text{screw}} = 16.85$ N
- $d = 0.003$ m(M3 nominal)
- t= effective local thickness of printed material around the hole

Using a conservative minimum recommended printed boss thickness:

$$t = 5\ \text{mm} = 0.005\ \text{m}$$

Then:

$$\sigma_b = \frac{16.85}{(0.005)(0.003)} = \frac{16.85}{1.5 \times 10^{-5}} = 1.12 \times 10^6 \text{ Pa} = 1.12 \text{ MPa}$$

Typical printed PLA compressive/bearing capability varies strongly with print settings; a conservative working allowable compressive stress for printed PLA can be taken as **~20–30 MPa** (depending on infill, layer adhesion, etc.). Using a conservative allowable of 25 MPa:

$$\text{FoS}_{\text{bearing}} = \frac{25}{1.12} \approx 22.3$$
$$\text{FoS}_{\text{bearing}} \approx 22 \text{ (with } t = 5 \text{ mm)}$$

Design note: Use **washers** and/or a **thicker boss** (≥5 mm) around screw holes to reduce local stress concentration and avoid creep.